Structural properties of softwood lignin fractions: Revealed by NMR and Py-GC/MS

Liu, Rui; Smeds, Annika; Willför, Stefan; Xu, Chunlin

Published in:
Industrial Crops and Products

DOI:
10.1016/j.indcrop.2024.118055

Published: 01/03/2024

Document Version
Final published version

Industrial Crops & Products 209 (2024) 118055

Contents lists available at ScienceDirect

Industrial Crops & Products

journal homepage: www.elsevier.com/locate/indcrop

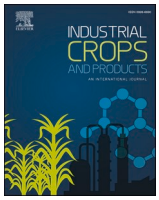

Structural properties of softwood lignin fractions: Revealed by NMR and Py-GC/MS

Rui Liu, Annika Smeds, Stefan Willför, Chunlin Xu *

Laboratory of Natural Materials Technology, Faculty of Science and Engineering, Åbo Akademi University, Henrikinkatu 2, 20500 Turku, Finland

ARTICLE INFO

Keywords:
Softwood kraft lignin
Structural properties
Kraft delignification chemistry
NMR
Py-GC/MS

ABSTRACT

The structural complexity of industrial softwood kraft lignin (ISKL) strongly interrelates to the heterogeneous chemical reactions of kraft delignification process. In this work, structural properties of an ISKL were revealed by the investigation on the structural properties of fractions with gradient molar mass and trace/high amount of carbohydrates. Moreover, the variation in structural composition of ISKL enables its classification into three distinct categories, which potentially correspond to the the lignin dissolved at different phases of kraft delignification. In general, the low molar mass fraction, characterized by an abundance of reduced subliknages and a minimal presence of native linkages, are tentatively associated with the lignin dissovled at the inital phase of delignification. The medium molar mass fractions with trace amounts of carbohydrates, exhibiting similarities in the quantites of β-O-4, benzyl ether (BE), and β-5 linkages, are probably dissolved into kraft liquor in the period of the bulk phase of delignification. The lignin fraction with the highest molar mass, containing a large amount of native sublinkages and carbohydrates, is correlated with the lignification phase toward the late of delignification. This study of structural characteristics of lignin fractions and their relationship to kraft delignification chemistry is anticipated to facilitate the separation of lignin to fractions with significantly reduced structural heterogeneity, thereby enhancing the potential for high-value application based on their compositional structure.

1. Introduction

Alternatives based on sustainable materials are in burning demand to fight against the predictable shortage of non-renewable petroleum-based products. (Beaucamp et al., 2022) Biomass of woody plants provides huge potential in providing raw materials (cellulose, lignin, hemicellulose, and extractives) for sustainable production of industrial products, chemicals, and medicines, etc. (Edgar et al., 2001; Farhat et al., 2017; Hansen and Plackett, 2008; Seabra et al., 2018) Lignin, the most abundant aromatic biopolymer on earth, has attracted extensive attention because of its vast potential applications in, e.g., pharmaceuticals, carbon precursor source, and for the production of aromatic chemicals. (Figueiredo et al., 2018; Liu et al., 2020; Nguyen et al., 2018; Upton and Kasko, 2016). Therefore, considering the value-added product based on lignin are welcome, a suitable fraction of lignin in a pulp and mill would be welcome for generating the value-added products. However, due to the structural complexity of various types of lignin, its application in value added products is still limited although millions of tons of lignin are annually produced. (Rodrigues et al., 2021).

Technical kraft lignin, available in bulk, is a byproduct of pulp production through the kraft process, (Dessbesell et al., 2020) among which more than 50% are derived from softwood kraft pulping. (Gellerstedt, 2015) Softwood lignin, which contains predominantly guaiacyl-propane units as the building blocks, is acknowledged to have a more homogenous structure and offers more advantages in the production of chemicals, such as vanillin, as well as in the production of stabilized lignin fibers. (Gellerstedt, 2015) However, industrial softwood kraft lignin (ISKL) is generally burnt in the pulping industry as energy for steaming, heating, and chemical recovery rather than being utilized for the development of higher added-value products due to the complex and ill-defined structure. (Dessbesell et al., 2020) Because structure of ISKL undergoes drastic changes during kraft cooking due to the heterogeneous reaction activities of native lignin moieties and the complex delignification chemical environments. (Dimmel and Gellerstedt, 2010) Therefore, an fundamental understanding of the structural architecture of ISKL is urgently needed in order to facilitate the future development of downstream products with added-value based on their inherent structural properties.

* Corresponding author.
E-mail address: chunlin.xu@abo.fi (C. Xu).

https://doi.org/10.1016/j.indcrop.2024.118055
Received 25 September 2023; Received in revised form 6 December 2023; Accepted 7 January 2024
Available online 16 January 2024

Fractionation of ISKL is a necessary step for studying its structural architecture and upgrading lignin into high-value-added products. Mainstream research on the general properties of kraft lignin typically involves characterizing the pre-fractionated lignin fractions that are obtained through membrane-based ultrafiltration or solvent fractionation techniques, including single-step and sequential extraction, pH-dependent precipitation, and fractional precipitation. (Gigli and Crestini, 2020; Sadeghifar and Ragauskas, 2020) Thanks to various approaches for lignin fractionation and advanced characterization techniques, the general properties of partial fraction of ISKL have been elaborated. Particularly lignin fractions with small molar mass tend to have the following properties: abundant in phenolic hydroxyl groups, (Alekhina et al., 2015; Cui et al., 2014; Liu et al., 2021) good solubility in organic solvents, (Novo and Curvelo, 2019; Schuerch, 1952) a low frequency of native linkages, (Giummarella et al., 2020) a moderate amount of condensed structure, (Chakar and Ragauskas, 2004; Gellerstedt, 2015) poor thermal stability, (Liu et al., 2022; Wang et al., 2018) etc. These elaborated properties are meaningful to optimally develop down-stream products based on the ISKL fraction with low molar mass. Thus, advocating for the reduction of heterogeneity in ISKL is widely recommended to develop value-added products based on internal variability in chemical and structural properties as well as molar mass.

However, reducing the heterogeneity of industrial lignin remains a vague academic term in lignin fractionation as there is no clear criterion for evaluating the heterogeneity degree of a lignin fraction due to the complexity of industrial lignin and the diversity of approaches used for lignin fractionation. Different fractionation methods aimed at reducing the heterogeneity of lignin also bring challenge to standardize the heterogeneity degree of a lignin since the general properties of the obtained lignin fractions, depending on the fractionation methods, can vary drastically even on the same batch basis. The fundamental cause of the extreme heterogeneity of ISKL originates from the complex structure of the native lignin and the heterogeneous delignification chemical reactions during kraft cooking.

In our previous work, (Liu et al., 2022) we proposed a solvent extraction approach for the separation of lignin fraction almost without carbohydrate and the fraction containing carbohydrates. Additionally, different fractions were further obtained based on their molar mass gradient. The in-depth structural analysis reveals a potential correlation between the fractions and the chemistry during different delignification phase, which may facilitate lignin fractionation depending on their structural architecture. In this study, the relationship between different lignin fractions and delignification chemistry is discussed, with a particular focus on the composition content of native lignin linkages, β-aryl ether (β-O-4), resinol (β-β), and phenylcoumaran (β-5), as well as the number of reduced linkages involving stilbenes (SB) and enol ether (EE) within each fraction.

2. Material and experimental

2.1. Lignin fractionation

Kraft lignin (UMP BioPiva 350) was fractionated according to our earlier report. (Liu et al., 2022) Simply, lignin was firstly washed by acidic water (pH 2.5), distilled water in turn to remove water-soluble substances, and then freeze-dried prior to solvent fractionation. The freeze-dried lignin powder was extracted by methyl *tert*-butyl ether (MTBE) to remove extractable substances (MTBE fraction), which consists of fatty acids, rosin acids, and phenolic substance, and low molar mass lignin oligomers. After that, the lignin sample was extracted by acetone (HPLC grade) to separate the acetone-soluble fraction that only with trace amount of carbohydrates (almost free of carbohydrates), and the acetone-insoluble fraction that with a large amount of carbohydrates. Then, the acetone soluble fraction was sequentially extracted by ethyl acetate (EtOAc), ethanol (EtOH), and methanol (MeOH) to obtain four fractions TC1 (by EtOAc), TC2 (by EtOH), TC3 (by MeOH), and TC4 (MeOH insoluble). Besides, three fractions with a higher contents of carbohydrates were obtained by sequential solvent extraction of EtOH, MeOH, and THF in order from the acetone insoluble fraction, namely, HC1 (by EtOH), HC2 (by MeOH), and HC3 (by THF). HC1 and HC2 are not discussed due to their low yields. Serval essential features of each lignin fraction are displayed in Fig. 1, more details about fractionation approaches, and the characteristics of these factions can be found in our previous report.(Liu et al., 2022).

2.2. Py-GC/MS and TMAH/Py-GC/MS experiments

Conventional pyrolysis: The pyrolysis gas chromatography-mass spectroscopy (Py/GC−MS) experiment was conducted using a Pyrola 2000 pyrolyzer coupled with Agilent GC 7890B system, and Agilent 5977B mass selective detector. 100 μg of each lignin fraction was transferred onto the platinum filament, which was then automatically inserted into the pyrolysis chamber. The chamber was maintained at 170 °C and purged with helium at a flow rate of 20 mL/min. Isothermal pyrolysis of each sample was carried out at temperatures of 350, 450, and 550 °C with a residence time of 2 s. The injector temperature of the GC system was set at 280 °C. The volatile compounds were separated by a capillary column (ZB-35, 30 m × 0.25 mm (L × I.D.)), with a film thickness of 0.25 μm) and helium as carrier gas at a flow rate of 8.0 mL/min. The temperature of capillary column was programmed as follows: initially set at 50 °C (held for 0.5 min), gradually increased to 320 °C with a heating rate of 8 °C/min, and then maintained for 4 min. A modified version of the Agilent ChemStation software, along with mass spectra databases including Wiley 11th, NIST 2012, and the one developed by the Laboratory of Natural Materials Technology (Åbo Akademi University) since 1970 s were utilized for identification of the recorded substances. The pyrolysis of lignin in the presence of tetramethylammonium hydroxide (TMAH Py/GC−MS) experiment was conducted using the same instrument. For TMAH Py/GC-/MS, 100 μg of each lignin fraction dissolving in 10 μL of TMAH solution (25% in methanol) was loaded onto the Pt filament and pyrolyzed at 360 °C for 2 s. The column temperature profile was the same as that used in conventional Py-GC/MS.

2.3. NMR experiment

Multiplicity edited heteronuclear single quantum coherence spectroscopy (HSQC) experiment: The HSQC experiments were performed using standard Bruker pulse sequence "hsqcedetgpsisp2.3″and 80 scan at 298 K on Bruker 500 MHz instruments. Lignin dissolved at a concentration of 0.12 mg/μL was used for scan. All data were processed with TopSpin software (version 4.0.6, Bruker). ^{13}C-Quantitative NMR: Bruker 500 MHz instruments with BBO Cryprobe system was used. 200 mg lignin sample was first dissolved in 0.49 mL DMSO-d_6, then 60 μL Chromium (III) acetylacetonate ($Cr(acac)_3$, 50 mg/mL in DMSO-d_6) was added to lignin solution to provide complete relaxation of all nuclei. The spectra were recorded by following procedure: an inverse-gate proton decoupling pulse program (*zgig*), spectral width 35714 Hz (−40–240 ppm), an acquisition time of 1.1 s, and a relaxation delay of 2 s, number of scan 20 000 times.

3. Results and discussion

3.1. NMR

The saturated aliphatic region of the HSQC spectra typically consists of various peaks presenting reduced lignin side chains and extractives. GC-MS results of MTBE fraction reveals significant proportion of fatty acids (4.99%), rosin acids (29.88%), phenyl/guaiacyl- units (15.57%), stilbenes (26.07%) and secoisolariciresinol (2.90%) (Table S1). Consequently, a substantial number of non-lignin related crosspeaks can be observed in the HSQC spectra of MTBE fraction (Fig. S1). The common

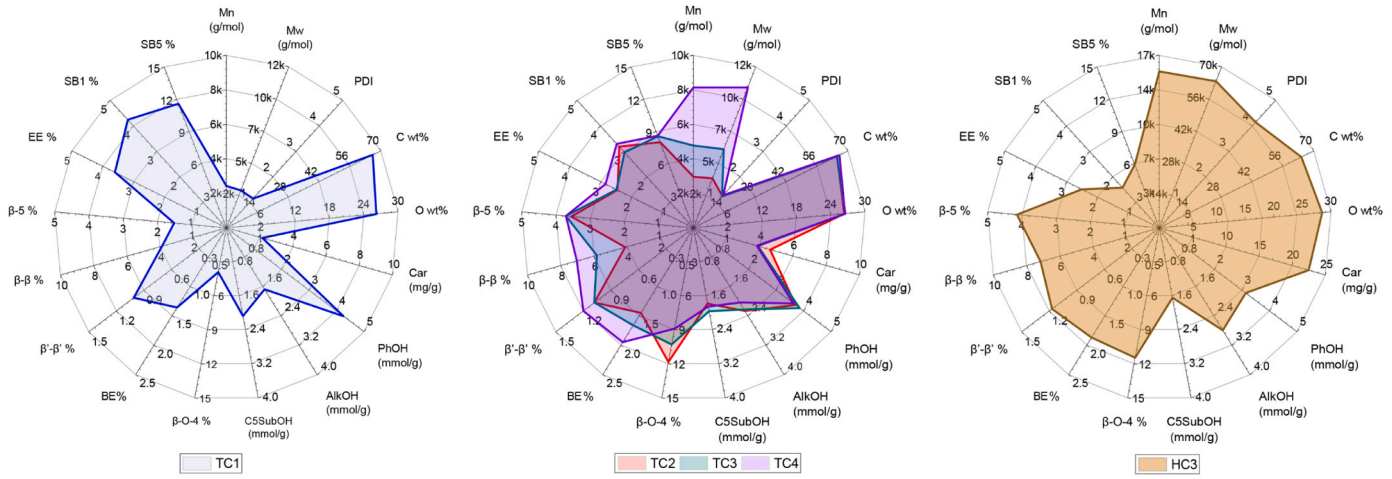

Fig. 1. Summary of key properties of TC1 (left), TC2, TC3, TC4 (middle), and HC3 (right) involving number average molar mass (Mn), weight average molar mass (Mw), polydispersity index (PDI), content of carbon (C), oxygen (O) in weight percentage, content of carbohydrates (Car) based on acid methanolysis method; content of phenolic (PhOH), aliphatic hydroxyl group (AlkOH), and C5-substituted hydroxyl group (C5SubOH); and semiquantitative abundance of selected lignin linkages in each lignin fraction (as per 100 aromatic units based on HSQC), β-aryl ether (β-O-4), benzyl ether(BE), epiresinol (β'-β'), resinol (β-β), phenylcoumaran (β-5), enol ether(EE). stilbenes (SB1 and SB5).

sublinkages, namely secoisolariciresinol (SR), guaiacyl- hydroxyethyl ketone (GHK), dihydrocinnamyl alcohol (DHCA), and guaiacyl- methyl ketone (GMK), are assigned based on the documented chemical shift data, Fig. 2(a). (Crestini et al., 2017; Lancefield et al., 2018) Note that TC1 presents high positive signals in number than TC2–4 and HC3. However, the overlapping HSQC spectra of MTBE fraction and TC1 in Fig. 2(b) suggest that some of the cross-peaks may originate from fatty acids or rosin acids, considering these compounds are captured from TC1 by TMAH Py-GC/MS). Given the fact that only a negligible amount of extractives may remain in lignin after MTBE extraction, it would be unreasonable to attribute the positive cross peaks, marked with red circles, within the range of δC/δH, 12–20/2.4–1.75 ppm as extractable substances. (Crestini et al., 2017) The presence of isoeugenol (2-methoxy-4-propenylphenol), a well-documented byproduct resulting from the kraft cooking of softwood, is also identified from the MTBE fraction through GC/MS analysis. Furthermore, significant amounts of isoeugenol have been detected in the pyrolysates obtained at temperature of at 350 and 450 °C via Py-GC/MS. Additionally, moderate quantities of methylated isoeugenol (4-(1-propenyl) veratrol) are observed when pyrolysis is conducted in the presence of TMAH. Therefore, it can assume that reduced end linkage of guaiacol prop-1-ene structure should be produced during kraft cooking. This presumption is supported by the partially overlapping HSQC signals observed for a cis/trans-isoeugenol mixture and lignin fraction, as the diagram inserted in Fig. 2(b). Additionally, the positive cross-peaks marked with red circles, linkages of GMK, and GHK are absent in the spectra of HC3 Fig. 2(a). The absence of these correlation peaks may be attributed to the decreased content of lignin linkages with reduced side chain, or a lower resolution of HSQC NMR for high molar mass lignin fractions.(Lancefield et al., 2018) The negative signal located at δC/δH = 29/3.8 ppm is commonly attributed to diarylmethane (DAM), a condensed lignin substructure found in ISKL. (Gellerstedt and Zhang, 2001; Lancefield et al., 2018) The significant variation in peak intensity of this cross-peak suggests the DAM moieties are predominantly present in TC1 and MTBE fraction, which correspond to fractions with lower molar mass. The uneven distribution of DAM substructure among these lignin fractions can be correlated to the heterogeneous chemical reactions involved in delignification and varying activities of native lignin moieties, which will be further discussed in this work. The additional negative signals of HC3, colored in black, are likely to originate from residue solvent as these signals cannot overlap with neither those negative signals of MTBE fraction nor the raw lignin with any treatment, Figs. 2(c) and 2(d). In summary, a comparison of the saturated aliphatic region in the HSQC spectra of each fraction indicates significant difference in structural composition between HC3 and TC1–4.

The oxygenated aliphatic and aromatic region of the HSQC spectra are shown in Fig. 3. Serval authorized native interlinkages can be observed among these fractions Fig. 3(a), including β-aryl ether (β-O-4, A, δCα/δHα = 71.23/4.82 ppm), phenylcoumaran (β-5, B, δCα/δHα = 86.53/4.64 ppm), resinol (β-β, C, δCα/δHα = 84.60/4.64 ppm), and cinnamyl alcohol (CA, δCγ/δHγ = 61.39/4.11 ppm) as reported in previous works. (Crestini et al., 2017; Lancefield et al., 2018) Noteworthy, ongoing debates still exist regarding the assignment of the cross peak at δC/δH = 80.89/4.76 ppm, which has been assigned as a benzyl ether (BE) structure within lignin carbohydrate complexes (LCC),(Crestini et al., 2017) or an epiresinol structure in previous reports. (Lancefield et al., 2018) However, these attributions contradict our observations. On one hand, the low content of residual carbohydrates within TC1–4 limits the detection of carbohydrate-related signals by HSQC spectroscopy, (Liu et al., 2022) suggesting that if this linkage were indeed a BE linkage, it would likely originate from the α-O-ethers of a non-phenolic structure, (Mattsson et al., 2017) rather than a benzyl ether associated with LCCs. On the other hand, cross peaks corresponding to epiresinol (β′-β′) have been reported at δC/δH = 80.89/4.76, 86.53/4.35 ppm (C′α/H′α), δC/δH = 53.66/2.85, 49.17/3.37 ppm (C′β/H′β), and δC/δH = 68.72/3.75, 68.68/3.13 ppm (C′γ/H′γ). (Lancefield et al., 2018) In this work, we observed a significant reduction in intensity for the C′β/H′β signal which is inconsistent with the assumption that different -CH- correlation peaks corresponding to one specific linkage should be proportional to its absolute amount in the sample volume-wise. Moreover, C′γ/H′γ cross peaks almost disappeared in TC4 and HC3 fractions while C′α/H′α and C′β/H′β could still be detected. This indicats that epiresinol may serve as an epimerization product derived from resinol structures under alkaline catalytic conditions and is more likely to be present in fractions with low molar mass. (Lancefield et al., 2018) Our observation aligns with this explanation, as evidenced by the significantly stronger intensities of C′γ/H′γ at 68.72/3.75 and 68.68/3.13 ppm in MTBE fraction and TC1 compared to those of TC2–4 and HC3 (Fig. S2).

Various substructures containing guaicayl- units, such as cinnamyl alcohol, cinnamaldehyde, E/Z-enol ether (EE), vanillin, guaiacyl methyl ketone, and stilbenes (SB1 and SB5) can be observed from the aromatic region in Fig. 3(b). The reduced sidechain due to formation of stilbenes and vinyl ethers is one of the most typical features of ISKL. Semiquantitative results (Table 1) indicated that TC1 has the largest number

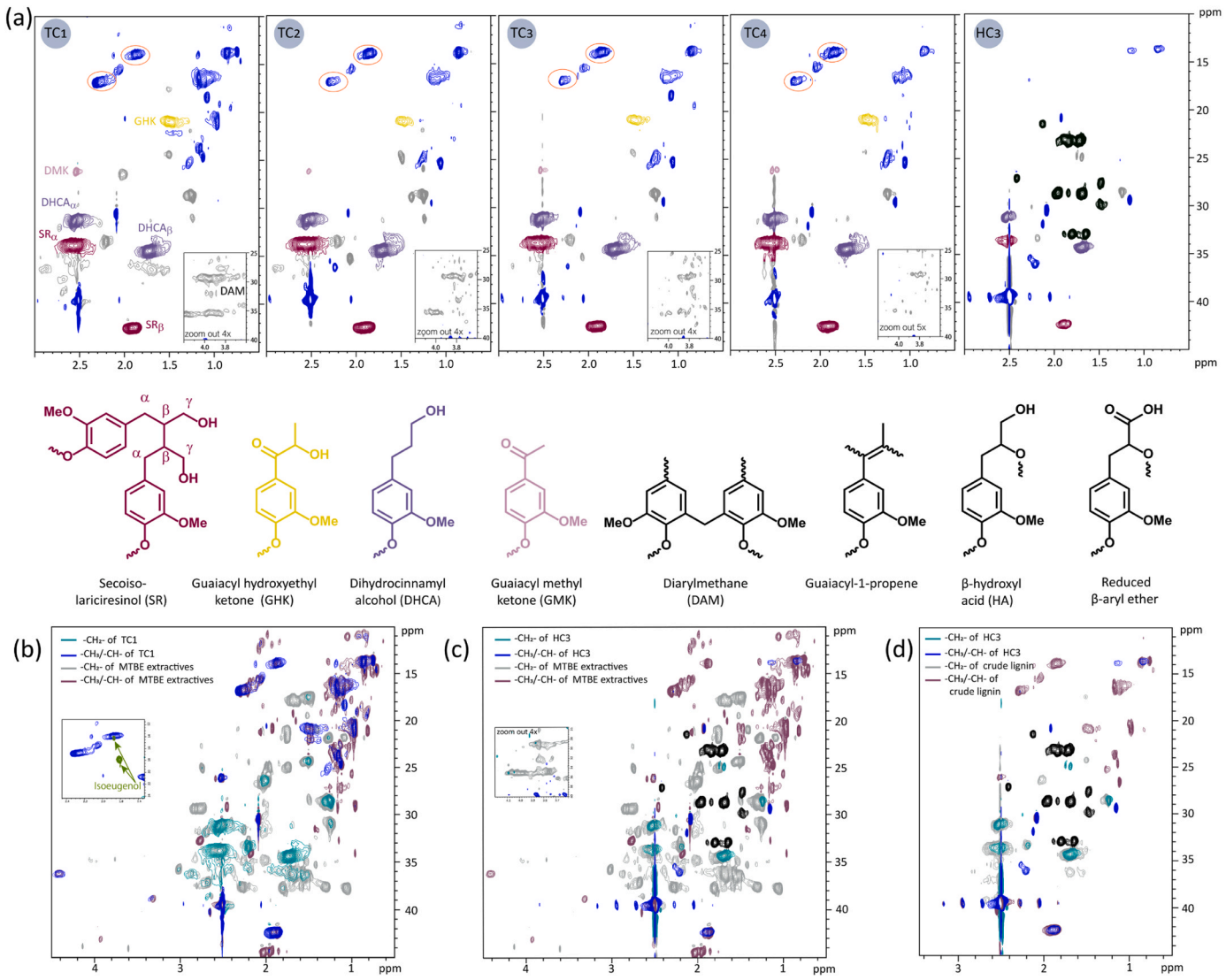

Fig. 2. (a) HSQC spectrum of the saturated aliphatic region of each lignin fraction, the unattributed blue cross-peaks are -CH_3 or -CH-. (b) overlapped HSQC spectra of MTBE fraction and TC1, inserting with overlapped spectra of isoeugenol and TC1, (c) overlapped HSQC spectra of MTBE fraction and HC3, inserting with overlapped cross peak region of diarylmethane (DAM) that from MTBE fraction and HC3, and (d) overlapped HSQC spectra of HC3 and raw lignin.

of reduced substructures : 11.58% of SB5, 4.24% of SB1 and 3.61% of enol ethers, while the survived native linkages, 3.92% of β-O-4, 3.88% of β-β, and 1.52% of (β-5) are lower than the counterparts in other fractions. In terms of fraction TC2–4, the content of each mentioned linkage above is quite similar in quantity except for the increasing trend of β-β and a slight decrease of β-O-4. The notable difference is that HC3 has significantly higher amounts of native sublinkages compared to TC1–4, while SB1 and SB5 structures are of the lowest levels. This interesting observation warrants further analysis of the structural composition of kraft lignin.

Condensed structure of lignin refers to lignin containing alkyl or aryl substituents at C5 and/or C6 position of the aromatic ring, such as β-1, β-5, 5–5, and 4-O-5 in native wood lignin. (Froass et al., 1998) Moreover, under alkaline pulping condition, the phenolic fragments of lignin are susceptible to condensation reactions, which lead to the formation of stable C-C linkages through a pathway involving carbanion addition to a quinone methide or formaldehyde addition to two phenolic rings with free C5 position of guaiacyl units. (Chakar and Ragauskas, 2004). Therefore, it is rather necessary to know the degree of condensation (DoC) of each fraction for a comprehensive investigation into their structural properties. Quantitative ^{13}C NMR spectroscopy is used to evaluate the DoC according to a previous report, where $DoC(\%) = (3G - C_{ArH}) \times 100\%$, (Tricker et al., 2020) The G is provided by the normalized integral of the methoxy peak (-OCH_3), since -OCH_3 is the primary substituent at C3 position of the guaiacyl- units;. C_{ArH} represents the normalized integral of aromatic carbons bonded to hydrogen. The peak area ranging from 162–102 ppm is calibrated to 6, and divided into 3 parts based on C5 substitution: aromatic carbons bonded to hydrogen (C_{ArH} $\delta = 125 - 102$ ppm), aromatic carbons bonded to carbon (CArC; $\delta = 142 - 125$ ppm), and the aromatic carbons bonded to oxygen (CArO; d=162–142 ppm), as shown in Fig. 4. The contribution of signals from conjugated double bonds in this region is disregarded due to their small quantity. The results suggest that the DoC among these fractions appear similar, except for HC3 with a DoC of 47.97% (Table 2). However, it should be noted that the reliability of HC3′s DoC may be compromised by its high polydispersity, and increased viscosity when dissolved in DMSO-d_6, which could potentially result in poor resolution in ^{13}C NMR analysis.(Lancefield et al., 2018; Landucci, 1991).

3.2. Py-GC/MS

A challenge associated with Py-GC/MS experiment is the intricate

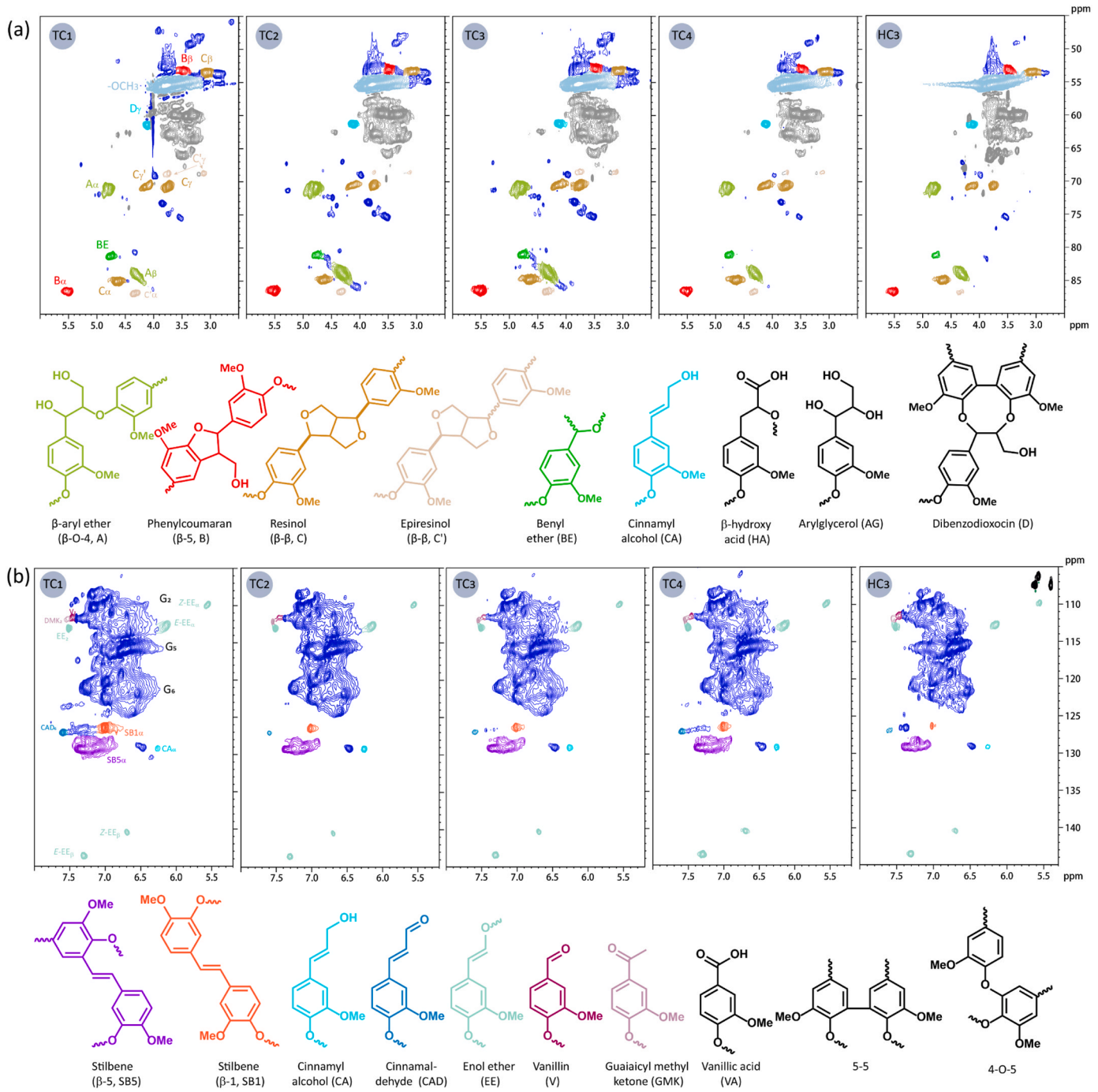

Fig. 3. HSQC spectrum of each lignin and assignments of the coloured structural features: (a) oxygenated aliphatic region and (b) aromatic region of each fraction. The unattributed blue cross-peaks are -CH_3 or -CH-.

temperature dependency of pyrolysis products. Primary pyrolysis reactions of lignin occur within a temperature range of 200–400 °C, during which α- and β-ether bonds are readily cleaved without affecting the O-CH_3 bonds through the study of liginn model compound. (Kawamoto, 2017) Considering the potential variations in thermal degradataion behavior arising from structural differences, the pyrolysis products of each fraction at 350, 450, and 550 °C are identified and listed in Table S2 to S5. When subjectd to pyrolysis at a temperature of 350 °C, the predominant volatile products are position 4-substituted guaiacols (2-methoxyphenol) derived from guaiacyl units (G), including *trans*-isoeugenol (G-CH=CH-CH_3), vinylguaiacol (G-CH=CH_2), dihydroconiferyl alcohol (G-CH_2-CH_2-CH_2OH), homovanillin (G-CH_2-CHO), vanillin (G-CHO), 4-eugenol (G-CH_2-CH=CH_2, coniferyl alcohol (G-CH=CH-CH_2OH) and cis-isoeugenol. Moreover, the total abundance of released compounds by each fraction suggests that TC_1 has lower thermal stability than TC2–4 and HC3, Fig. 5(a). This result is consistent with previous studies, where obeserved that lignin fractions with a low molar mass exhibited thermal unstability. (Liu et al., 2022; Wang et al., 2018) However, considering the minimal disparity in molar mass between TC1 (Mn 2419, Mw 2788, g/mol) and TC2 (Mn, 2961, Mw 3687 g/mol), it can be inferred that the observed results is likely attributed to the diversity and quantity of linkages within each fraction rather than soly relying on molar mass, at least within these two fracitons. The increase in pyrolysis temperature induces sencondary

Table 1
Semiquantitative abundance of selected lignin linkages in each lignin fraction (as per 100 aromatic units).

Linkages	HSQC Abundance (%)[a]					Chemical shift for integration (ppm)
	TC1	TC2	TC3	TC4	HC3	
β-aryl ether (β-O-4)	3.92	11.86	10.31	8.92	11.47	71.23/4.82 (Cα-H)
Benzyl ether	1.36	1.45	1.66	1.95	1.87	80.89/4.76 (Cα-H)
Epiresinol (β'-β')	1.01	1.08	1.08	1.20	1.17	86.53/4.35 (Cα-H)
Resinol (β-β)	3.88	4.11	5.82	7.02	7.17	84.60/4.64 (Cα-H)
Phenylcoumaran (β-5)	1.52	3.56	3.71	3.71	4.15	86.29/5.52 (Cα-H)
Secoisolariciresions (β-β)	3.15	4.07	3.52	3.19	3.86	42.22/1.91 (Cβ-H)
Dihydrocinnamyl alcohols[b]	3.30	3.96	3.97	3.76	4.29	34.32/1.40 (Cβ-H)
Cinnamyl alcohol	1.12	1.78	1.96	1.85	2.70	61.39/4.11 (Cγ-H)
Enol ether	3.61	2.46	2.49	2.85	2.51	119.92/6.14 (Cα-H)
Stilbenes (SB1)	4.24	3.19	2.96	3.30	1.58	125.61/6.99 (Cα-H)
Stilbenes (SB5)	11.58	7.98	8.53	8.59	5.91	128.97/7.05 (Cα-H)

[a] The abundance of lignin linkages structure were based on the integrated relative to the aromatic G2 position set to 100 (δ_C / δ_H 109-113/6.9-7.3) ppm; [b]-CH_2-divided by 2.

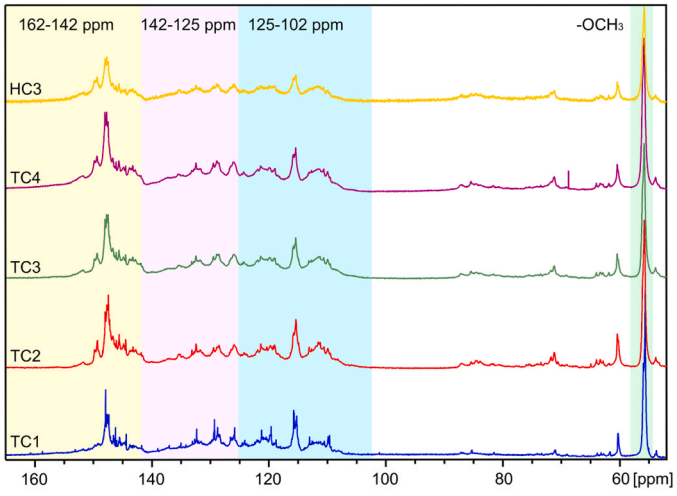

Fig. 4. ^{13}C NMR spectra of each lignin fraction. The highlighted region describes the integration boundary of methoxy carbons (-OCH_3, 58–54 ppm), aromatic carbons bound to oxygen (CArO, 162–142 ppm), aromatic carbons bonded to carbon (CArC, 142–125 ppm), and aromatic carbons bound to hydrogen (CArH, 125–102 ppm).

Table 2
Integral values of the ^{13}C NMR spectra. Integral values were normalized by defining the sum of the three aromatic regions as 6.

Sample	-OCH_3 58-54 ppm	C_{ArO} 162-142 ppm	C_{ArC} 142-125 ppm	C_{ArH} 125-102 ppm	CoD
TC1	0.8530	1.6654	1.9728	2.3618	19.72%
TC2	0.8779	1.7195	1.7855	2.4990	13.47%
TC3	0.8185	1.8216	1.8621	2.3163	11.10%
TC4	0.9684	1.0884	2.2060	2.7056	19.96%
HC3	0.9434	1.8565	1.7930	2.3505	47.97%

pyrolysis reaction, resulting in the cleavage of C-C bonds on the side chains. This enchances the production yield of monomers containing various alkyl side chains, including unsbstituted guaiacol, 4-methyl guaiacol (G-CH_3), 4-ethyl guaiacol (G-CH_2-CH_3), guaiacyl-propyl-3-ol (G-CH=CH-CH_2OH), and others as shown in Fig. 5(b). At the same time, the cleavage of the O nol. These phenomena are evident in all lignin fractions undergone pyrolysis at 450 and 550 °C.

The prevailling perspective suggests that the thermal stability of lignin is significantly influenced by its molar mass. However, it should be emphasize that the distinct thermal stability of different fractions are determined by their variable architecturue in essence. The reported bond dissociation energies (BDEs) of C-O within the main interlinkage groups at the side chain are as follows: α-O-4 (48.45–57.28 kcal mol^{-1}), β-O-4 (56.54–72.30 kcal mol^{-1}), 4-O-5 (77.74–82.54 kcal mol^{-1}), β-β (65.07–82.93 kcal mol^{-1}), and C-C BDE of β-5 (102.05–104.92 kcal mol^{-1}), β-1 (125.2–127.6 kcal mol^{-1}), and 5–5 (114.9–118.4 kcal mol^{-1}). (Shen et al., 2020; Supriyanto et al., 2020) These values indicate that cleavage of α- and β-aryl ether bonds dominates the thermolysis process at a low temperature, while with increasing temperature, the dissociation of 4-O-5, β-β, and C-C bonds becomes influential. The total ion abundance released by TC1 at 350 °C is nearly an order of magnitute higher than those of other fractions, indicating that a short macromolecular chain of TC1 may have significant number of untable bonds such as α- and β-ether bonds linkage. And these bonds are not condensed with other thermally resistant linkages so that volatile compounds are released in quantity at a low temperature.

Additionally, the BDE of these sublinkages also suggests that the thermal stability of each lignin macromolecule could be enhanced by increasing amount of thermally stable sublinkages. The volume of the pyrolyzates, such as 4-methylguaiacol could be a reasonable marker to estimate the amount of phenylcoumaran (β-5) linkage. This is supported by the observation that during the pyrolysis of β-5 lignin model compound at 500 °C, 4-methyl guaiacol was the most abundant product, following by 4-ethyl guaiacol, and 4-vinyl guaiacol.(Kuroda and Nakagawa-izumi, 2006a) While model compounds of guaiacyl-glycerol-β-guaiacyl-ether and guaiacyl-glycol-β-propylphenyl indicated that β-aryl ether substructures were not the primary source for producing 4-methylguaiacol.(Kuroda, 1994; Kuroda and Dimmel, 2002) Additionally, the low yield of 4-methylguaiacol released from coniferyl alcohol benzyl ether suggests that 4-O-etherified coniferyl alcohol is unlikely to be the source of 4-methylguaiacol. (Kuroda, 2000) Based on the pyrolsis characteristics of different model compounds mentioned above, it can be inferred that the abundance of β-5 contributes to enhancing the thermal stability of lignin macromolecules, as evidenced by the increasing trend of β-5 by HSQC and the released 4-methyl guaiacol within each fraction.

The abundant resinol (β–β) is one of the key linkages that contribute to the prevalence of stable C-O ether bonds in softwood kraft lignin. (Zhang et al., 2003) Notably, the BDE of the C-O ether bond in pinoresinol model compounds exceeds that of the ether bonds in phenylcoumaran.(Elder, 2014) Furthermore, our observations indicate that pinoresinol exhibits excellent thermal stability and alkali resistance, as no additional products are observed even when pyrolyzed at a temperature of 650 °C and in the presence of TMAH at 360 °C. (Fig. S3). Thus, the presence of a β–β structure with alkali and thermal resistance within in lignin macromolecular can effectively mitigate the release of volatiles. The semiquantitiative results based on HSQC reveal that the thermally resistant fractions HC3 and TC2–4 contain a higher proportion of β–β and β-5 compared to TC1.

3.3. TMAH Py-GC/MS

A major drawback of the conventional pyrolysis is the loss of structural information caused by the fragmentation of the propane side chains and the poor chromatographic behavior of lignin monomers containing polar functional groups.(Klingberg et al., 2005)

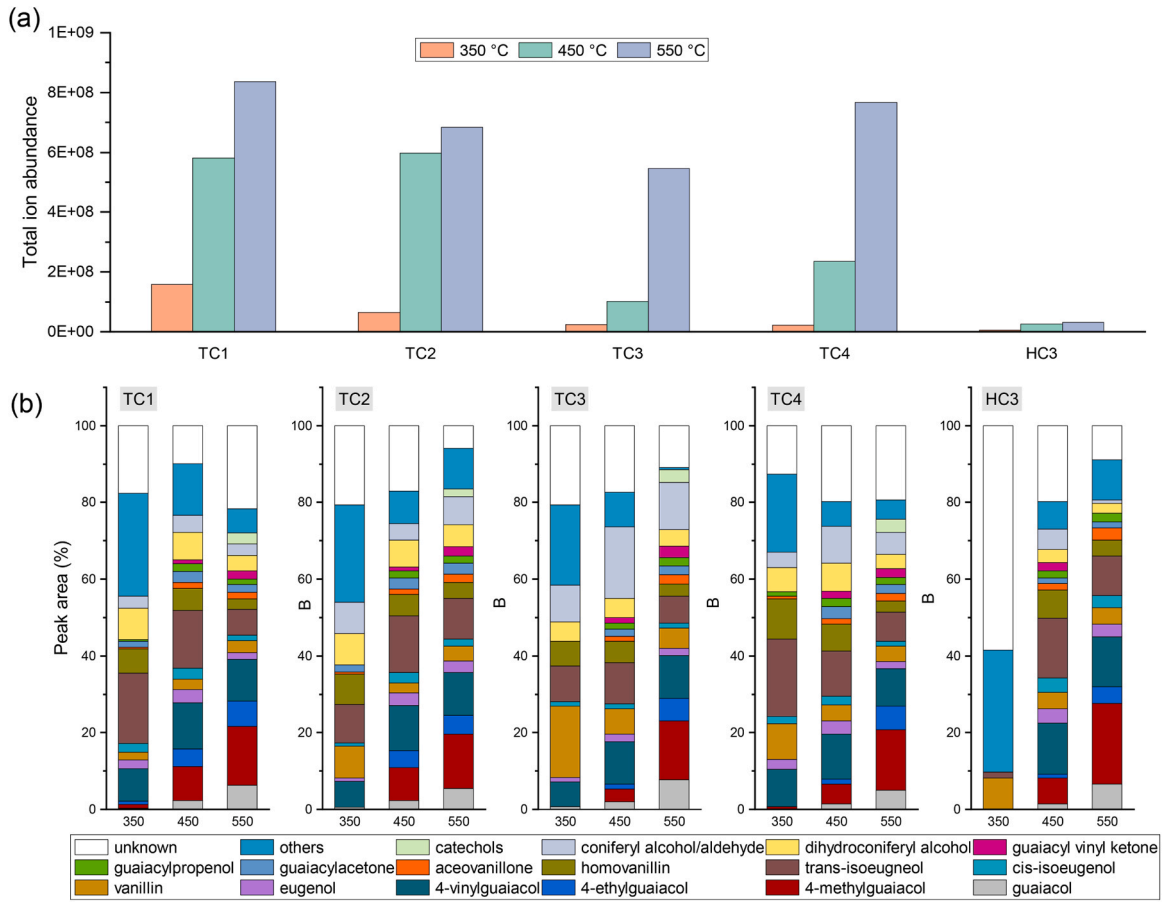

Fig. 5. (a)Total ion abundance of the volatile products from each fraction pyrolyzed at 350 °C, 450 °C, and 550 °C. (b) The main lignin relevant compounds produced from each fraction when being pyrolyzed at different temperatures, based on normalizing the GC/MS signal areas of the total identified peaks to 100%.

Thermochemolysis, empolying thermally assisted hydrolysis and methylation, is a well-established approach to overcome the shortcomings of conventional Py-GC/MS.(Challinor, 2001) TMAH Py-GC/MS is a unique in situ methylation technique, which can thermochemically drive a reaction between the carboxylic -OH, phenolic/aliphatic -OH. This process thus promotes the cleavage of chemical bonds such as esters and ethers within lignin. Additionally, it also facilates the alkylation of lignin, leading to the generation of alkyl esters and ethers.(Shadkami and Helleur, 2010) As a result, compared to conventional pyrolysis, less polar pyrolysates and higher yields of phenolic derivatives with more

Table 3
Peak assignment and their peak area percentage (% area) in the TMAH Py-GC/MS of each lignin fraction.

no	Compounds	Formula	TC1% area	TC2% area	TC3% area	TC4% area	HC3% area
1	Methyl veratrol	V-CH_3	na	0.32	0.92	0.68	na
2	4-vinylveratrol	V-CH_2 =CH_2	2.99	2.37	1.45	1.62	1.35
3	4-methoxyveratrol	V-OCH_3	3.59	1.62	0.31	2.27	1.75
4	Veratrylmethanol methyl ether	V-CH_2-OCH_3	6.55	4.49	0.52	5.03	5.05
5	4-(1-proenyl) veratrol	V-CH=CH-CH_3	1.25	0.65	3.44	1.13	0.67
6	Veratryl aldehyde (V-CHO)	V-CHO	1.41	2.86	1.36	1.47	na
7	Veraric acid me. ester	V-CO-OCH_3	7.88	4.16	8.68	11.90	0.42
8	3-veratrylpropan-1-ol, me. ether	V-$CH_2CH_2CH_2$-OCH_3	20.32	12.70	9.90	9.87	15.97
9	2-veratrylethen-1-ol methyl ether (cis)	V-CH=CH_2(OCH_3)	5.79	6.48	6.32	6.74	6.72
10	2-veratrylethen-1-ol methylether (trans)	V-CH=CH_2(OCH_3)	10.58	11.86	10.14	11.02	13.90
11	Veratrylprop-1-en-1-ol, methyl ether	V-C(OCH_3)=CH-CH_3	2.50	2.45	2.31	2.01	2.46
12	Veratrylprop-1-en-1-ol, methyl ether	V-CH(OCH_3)=$CHCH_3$	2.37	1.83	3.02	2.48	1.92
13	1-veratryl-1,3-propandiol, dimethyl ether	V-CH(OCH_3)-CH_2-CH_2(OCH_3)	1.96	1.05	1.00	1.12	1.04
14	(methoxy propenyl)-veratrol	V-CH=CH-CH_2OCH_3	4.36	3.92	4.78	5.10	4.39
15	veratrylglycerol trimethyl ether (*erythro*)	V-CH(OCH_3)-CH(OCH_3)-CH_2(OCH_3)	5.94	9.16	6.07	7.67	14.57
16	veratryl glycerol trimethyl ether (*threo*)	V-CH(OCH_3)-CH(OCH_3)-CH_2(OCH_3)	6.59	10.27	8.11	8.60	15.50
17	Stilbenes		0.15	0.26	0.34	0.29	0.76
18	Secoisolariciresinol, permethyl-		2.39	1.34	1.23	1.26	1.56
19	resin acids		0.16	0.56	0.28	0.65	0.53
	Unknown		13.22	21.65	29.82	19.09	11.44
	Total ion abundance (TIC)		4.96E+ 08	2.05E+ 09	1.75E+ 09	1.23E+ 09	1.17E+ 09

V-: veratryl (3,4-dimethoxyphenyl),
na: non-analyzed for its rather low yield.

detailed side chain of the lignin monomers are amenable to chromatographic analysis.(McKinney et al., 1995; Reale et al., 2004) During the thermochemolytic process, β-aryl ether linkages in lignin are effectively cleaved through alkaline hydrolysis at elevated temperature, accompanying elimination or subsequent methylation of oxygen functionalities, to yield compounds with veratryl- units (3,4-dimethoxyphenyl, V-). These compounds can have one, two, or three methoxy groups attached to the 4-substituted propanoids side chain of V- units.(Clifford et al., 1995; Tanczos et al., 1999) Other types of V- units, such as 4-vinylveratrol, 4-methoxyveratrol, veratryl aldehyde, and 2-veratrylethen-1-ol methyl ether, can also be released as the result of the delignification reaction during kraft cooking(Table 3).

The behavior of β-aryl ether subunits in TMAH Py-GC/MS is expected to be similar to that observed during alkaline pulping process. The free-phenolic units undergo the formation of quinone methide intermediates and subsequently transform into enol ether bonds, while the non-phenolic unit suffer from the cleavage of ether bonds to generates arylglycerol group.(Chakar and Ragauskas, 2004) The pyrolysis of a β-O-4 model compound, guaiacyl-glycerol-β-guaiacyl- ether, in the presence of TMAH resulted in the formation of veratrylethen-ol methyl ether, veratrol, and veratrylglycerol trimethyl ether. Moreover, they found that the formation of veratrylethen-ol methyl ether can be suppressed for non-phenolic β-aryl ether subunits.(Kuroda and Nakagawa-izumi, 2006b) In this study, *erythro/threo*-veratrylglycerol trimethyl ether and *cis/trans*-2-veratrylethen-1-ol methyl ethers are extensively liberated. The veratrylglycerol trimethyl ether represents the typical of the β-O-4 structure or the minimal amount of arylglycerol end group produced during kraft cooking, while the presence of latter is negligible according to HSQC results. The variation in total ion abundance of these compounds released by each fraction indicats a variation in the remaining quantity of the β-O-4 structure, which follows an order of HC3 > TC2 > TC4 ≈ TC3 > TC1 (Table 3). This trend aligns with the semiquantitative result of β-O-4 sublinkage based on HSQC. Moreover, a higher total ion abundance of 2-veratrylethen-1-ol also indicates that fraction HC3 may remain a large proportion of phenolic β-O-4 linkages.

In addition, a substantial quantity of 3-veratrylpropan-1-ol methyl ether is produced, potentially originating from dihydroconiferyl alcohol units that generated from the disproportionation reaction of coniferyl alcohol.(Fu and Lucia, 2004) The abundance of 3-veratrylpropan-1-ol methyl ether follows order of TC2 > HC3 ≈ TC3 ≈ TC4 >TC1, and this trend is consistent with the content of dihydroconiferyl alcohol according to the HSQC results. The higher percentage peak area of 3-veratrylpropan-1-ol methyl ether released from TC1 and HC3 suggests that sublinkages connected with dihydroconifery alcohol in these two fraction may be less resistant to TMAH themochemolysis within TC2–4.

Phenylcoumaran (β-5) linkages are usually subjected to a degradation pathway involving the elimination of formaldehyde from the γ-CH_2OH, resulting in the formation of stilbenes (SB5). (Kuroda et al., 2002) However, when the β-5 substructures are linked to more than one substructure through chemical bonds resist to TMAH thermochemolysis, the generated stilbenes become undetectable due to their non-volatile or larger molar mass. Thus, the captured stilbene may come from the existing stilbene linkages, or a β-5 structure connected with an unstable structure in the TMAH assistant thermochemolysis. A similar explanation could also be applied to resinol (β-β) linkage since TMAH pyrolysis at 360 °C is insufficient to break the C-O ether bonds in resinols, which often occur together with a 5–5 or a 4-O-5 linked structure.(Önnerud, 2002) The observation of a small number of permethyl-secoisolariciresinol should come from partial secoisolariciresinols that are connected to lignin polymer through β-O-4 bonds or other unstable linkages, which can be cleaved during TMAH thermochemolysis (Lapierre et al., 1991; Zhang et al., 2003).

3.4. Correlation between fractions and delignification chemistry

The complexity of kraft lignin is determined by both the inherent structure of native lignin and the heterogenous delignification reactions, which are influence by the concentration of cooking agents, sodium hydroxide (NaOH) and sodium sulfide (Na_2S), as well as the temperature in the course of kraft cooking.(Dimmel and Gellerstedt, 2010) In a standard pulping process, it shows three phases: an initial where 20–25% of the lignin can be dissolved at low temperature; a bulk phase where around 70% of lignin is dissolved at temperatures above 140 °C with increase in delignification rate due to increased temperature and sufiicient hydroxide/sodium sulfide; and the residue phase characterized by the reduce lignin concentration in the resulted fiber.(Dimmel and Gellerstedt, 2010) Among the various reactions of lignin fragmentation, the most two important pathways are the formation and subsequent reaction involving quinone methide intermediates, as well as the cleavage of β-aryl ether bonds through oxirane intermediates with involvement of neighboring ionized group, specifically hydroxyl group in the α- or β-position.(Gierer, 1985) Quinone methide intermediates constitute the rate-determining step in the reactions of phenolic lignin units and also contribute to the formation of various reduced linkages during kraft cooking.(Dimmel and Gellerstedt, 2010) For example, these intermediates are conducive to the production of enol ethers by a rearomatization pathway, which can involve either deprotonation of the β-carbon or reversal of aldol reaction by eliminating formaldehyde from the γ-carbon. Moreover, due to the facile reactivity of the unstable quinone methide intermediates, nucleophiles, such as HO^-, and HS^-, and anions of the phenolated by-product, can be added to the α-carbon of these intermediates for subsequent rearomatization, fragmentation and condensation, Scheme 1(a).(Dimmel and Gellerstedt, 2010) Besides, quinone methides are responsible for the cleavage of the sublinkages with β-1, β-5, and β-β to the formation of linkages with stilbenes, Scheme 1(b).(Dimmel and Gellerstedt, 2010) Additionally, diarylmethane linkages can be formed via condensation reactions of phenolic moieties under alkaline conditions. This process involves introducing a carbanion to quinone methide and/or adding of formadehye to two phenolic moieties with an unoccuppied C5 position, Scheme1 (c).(Dimmel and Gellerstedt, 2010) The quinone methide is usually formed by the departure of an anion from the α-carbon position of the phenolate anions in mo del compounds. Hence, the presence of native lignin linkages containing phenolic hydroxyl groups or ionized phenolates should be one of the prerequisites for the formation of quinone methide intermediates. In other words, the content of phenolic hydroxyl groups in both native and newly formed phenolate lignin linkages during the delignification process may be correlated with the number of reduced linkages.

During the initial phase of delignification, phenolic linkages readily undergo conversion into quinone methides involving the cleavage of α-aryl ether and of β-aryl ether linkages in phenolic units.(Gierer, 1985; Ljunggren, 1980) Teder et al. reported that approximately 20% of lignin was released as low molar mass fragments in this phase.(A.olm, 1981) Similarly, Gellerstedt et al. also observed that during the inital stage of kraft cooking, the lignin entering into the solution had a low molar mass and a large number of phenolic hydroxyl groups.(Gellerstedt and Lindfors, 1984) Additionally, the authors also noted a significant change in the structural composition of residual lignin in the pulp after the inital stage: the number of phenolic guaiacyl-terminal groups decreased rapidly, while the molar mass increased. This suggested that the dissolved lignin in the bulk phase differed somewhat from the initial counterpart.(Gellerstedt and Lindfors, 1984).

In this work, MTBE was used as an effective solvent for the removal of extractives and lignin/lignan-related monomers, dimers, trimers and oligomers.(Smeds et al., 2012) The molar mass of MTBE fraction was 934 g/mol for Mw and 523 g/mol for Mn. Partial compounds of MTBE fraction may represent reduced products of delignification in the initial stage, such as stilbenes, diarylmethane, and epiresinol that were identified by GC/MS or HSQC. Besides, among these fractions, TC1 exhibits the following characteristics: the lowest molar mass, the highest content of both phenolic and C5 substituted hydroxyl groups, and a considerable number of reduced linkages of SB5, SB1, EE, and DAM in comparison to

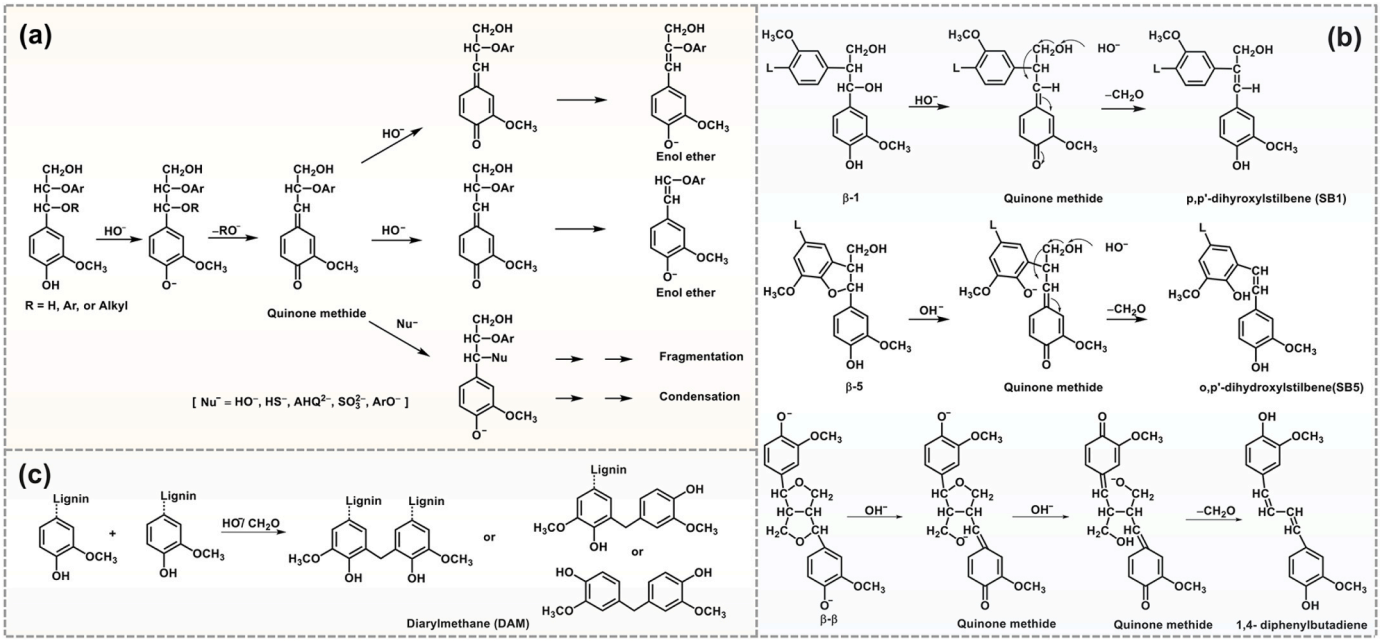

Scheme 1. (a) Formation of quinone methide intermediate from phenolic lignin linkage to produce enol ethers by rearomatization pathway. (b) Formation of stilbenes from β-1, β-5, and β-β lignin substructures in alkaline media. (c) The formation of diarylmethane structures.

fractions TC2–4 and HC3. These properties of TC1 may be correlated to the lignin fragments dissolving in the initial phase, where 1) extensive cleavage of phenolic units can accelerate the formation of fragments with low molar mass and abundant phenolic groups, and 2) a higher concentration of NaOH contributes to the cleavage of β-1, β-β, and β-5 linkage in phenolic units to the reduced linkage of stilbenes. During kraft cooking almost all types of β-1 structures were degraded. For example, a native spirodienone (β-1/α-O-α) linkage was readily transformed into an SB1 structure. (Gellerstedt et al., 2004; Lancefield et al., 2018) The absence of a distinct β-1 linkage signal in the HSQC spectra could potentially be attributed to this factor, as well as serving as a plausible reason for the disparity in SB1 quantities observed among TC1–4 and HC3. Similarly, a large quantity of SB5 linkage could be generated due to a preferential degradation of phenolic phenylcouraman linkage (β-5) in the initial phase. Consequently, the dissolved lignin in the inital phase contains a lower abundance of phenylcouraman linkages compared to those dissolved in later phases. In addition, DAM could be produced much easilier through condensation reaction because of the higher level of ionized phenolic linkages in the initial phase. These may be reasonable cause that the HSQC spectra of MTBE fraction and TC1 exihibit intensive cross peaks belonging to DAM. Besides, it has been suggested that at the transition point between initial phase and bulk phase, the transformation of β-aryl ether structure into enol ether structure decreased due to the shortage of HS^-. (Gellerstedt et al., 1984; Mattsson et al., 2017) Coincidentally, the content of enol ether structure (3.61%) in TC1 is slightly higher than TC2–4 and HC3 (2.46%, 2.49%, 2.85%, and 2.51%). Accordingly, it can preliminarily conclude that the extraction of lignin-related substances by MTBE and TC1 fraction reprsesent the lignin dissolved in the initial delignification phase.

As the cooking proceeds into the bulk phase, both softwood and model compounds demonstrated that the cleavage of β-aryl ether linkages in non-phenolic units was a key factor in determining the rate of the bulk delignification. (Gierer, 1985; Ljunggren, 1980) On the other hand, the concentration of HO^- is also rate determining factor for the cleavage of non-phenolic β-aryl linkages. Thus, the rapid consumption of HO^- would decelerate the cleavage of non-phenolic β-aryl ether linkages. Moreover, the subsequently insufficiency of HO^- is adverse to the cleavage of β-aryl ether, thus potentially leading to an elevated presence of β-aryl ether linkages within the lignin fragments. The cleavage trend of non-phenolic linkage of β-β, and β-5 may be similar to that of β-aryl ether because of their stronger thermal and alkaline resistance. Other studies conducted on structural changes of lignin during kraft cooking observed that the dissolved lignin in bulk phase presented higher molar, less abundant of phenolic group in comparison with those dissolved in the initial phase.(Dang et al., 2016; Gellerstedt and Lindfors, 1984; Mattsson et al., 2017) By focusing only on the number of typical native linkages (β-O-4, β-β, β-5, and BE), it shows that despite an increase in molar mass, the overall content of these native interlinkages within fractions TC2–4 remains relatively consitant at 20.98%, 21.50%, and 21.60%, respectively, while exhibiting values of 10.68% in TC1 and 24.66% in HC3. (Fig. 6). The improved resistance to kraft cooking of β-5, β-β, biphenyl 5–5, 4-O-5 may be a reasonable attribution to make TC2–4 have more similarities in structural archetectures.(Mattsson et al., 2017) It is worth noting that the content of the β-β (resinol) linkage shows an upword trend with the increase of molar mass of T2–4 and HC3, suggesting this linkage may be one of the most important ones in bridging different sublinkages.

The fragmentation of lignin into kraft liquor is also affected by the polysaccharides linked to lignin.(Gellerstedt, 2015) The types of carbohydrates that bond with lignin present different resistance behaviors to kraft cooking. Study conducted on the properties of the dissolved lignin during kraft cooking in a flow-through reactor has revealed an increase in both molar mass and LCC content of the dissolved lignin after 40 – 90 min of cooking.(Mattsson et al., 2017) Gellerstedt et al. obersverd that the materials dissolved contains xylose, together wtih some galactose and arabinose in the later delignification stage.(Gellerstedt and Lindfors, 1984) Lawoko et al. reported that, the majority of xylan-bound lignin is dissolved and degraded to a lower molecular mass fractions towards the later stage of kraft cooking, however, the glucomannan-linked lignin can still be observed on the residue fibers after the delignification.(Lawoko et al., 2004; Lawoko et al., 2005) Because the galactose-lignin bond is less susceptible to hydrolysis in alkaline conditions compared to a regular glycosidic bond,(Berglund et al., 2018) it is possible to presume that the galactose present in the side chains of galactoglucomannan may be primarily involved in the covalent bonding between hemicellulose and lignin.(Abbadessa et al., 2018).

One of the most striking features of HC3 is the detectable carbohy-

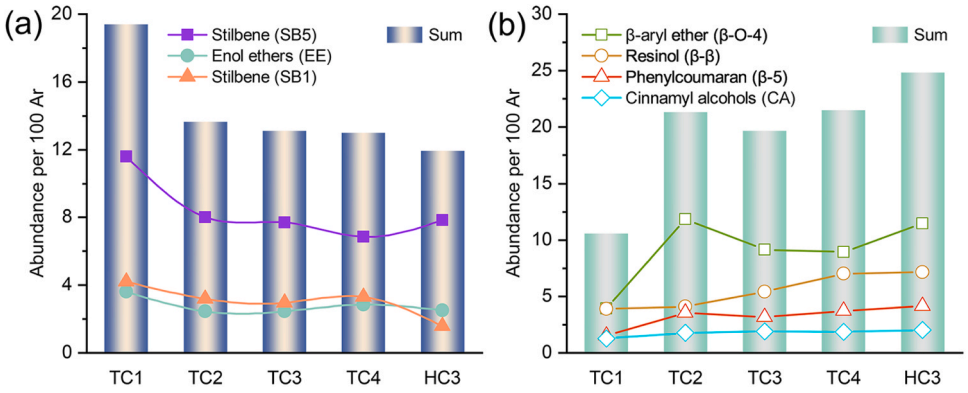

Fig. 6. Comparison of content of typical substructures, stilbenes and enol ethers, (a) and survived native linkages (β-aryl ether, resinol, phenylcoumaran, and cinnamyl alcohol); (b) in each lignin fraction based on the HSQC.

drates through analysis of its acid methanolysis solution, with galactose being the predominat neutral sugar moiety.(Liu et al., 2022) Incidentally, because of its carbohydrate content exceeding 10%, with xylose, arabinose, galactose and glucose being the major constituents, approximately 10% residue lignin (after HC3) could not be characterized owing to its poor solubility.(Liu et al., 2022) Besides, HC3 also contains a higher abundance of native linkages, β-5, β-β, and β-O-4 compared to other fractions. Mattsson et al. also suggested that partial β-O-4 linkages are stable enough to protect themselves from being cleavaged, even dissolved in the constant concentration of HO^- and HS^-. Morevoer, the native linkages of β-5, β-β, and β-O-4 in dissolved lignin can be maintained at a higher level as the cooking proceeds towards the end of the bulk phase.(Mattsson et al., 2017) Abundant β-5, β-β linkage of HC3 thus contribute to its high degree of condensation and increase its thermal stability consequently. Thus, the fraction contains evident carbohydrate and retains a substantial amount of native lignin linkages, probably derived from the late stage of delignification.

4. Conclusion

The structural composition of an industrial softwood kraft lignin allows for its classification into three categories: the low molar mass fraction (TC1) contains a significant amount of phenolic hydroxyl groups and reduced linkages of stilbenes and enol ethers; the moderate molar mass fraction with broad polydespersity (TC2–4) maintains relatively stable content of native linkage (β-O-4, β-5), as well as reduced sublinkages; and the higher molar mass fraction (HC3), which is primarily featured by carrying carbohydates, abundant native linkage, and a low level of reduced structures. Moreover, the properties of each fraction based on these categories are associated with the delignification phase of kraft cooking. During the faster initial delignification phase, phenolic lignin moieties with a higher activity may undergo severely degradation leading to the formation of low molar mass fraction comprising a large number of depolymerized structures and phenolic hyroxyl groups. The fractions dissolved into kraft liquor in the period of the bulk phase of delignification have a mederate molar mass and similar structural components content of both native and reduced linkages. The high molar mass fraction preserves large number of native linkages and carbohydrates is correlated to the dissolved materials toward the late stage of cooking. This study on the structural properties of lignin fractions and their correlation with delignification chemistry of kraft pulping would facilitate the separation of fraction-dependent linkage abundances and the optimum valorization of lignin in the future. However, more in-depth investigations are still required to elucidate the chemical reaction/structural composition/function of lignin dissolved at different delignification stage.

Author contribution

R.L performed the investigation, experiments, visualization of the data and writing of original draft. A.S. assisted in the Py-GC/MS and TMAH/Py-GC/MS experiments. C.X. provided funding and resources and supervised the investigation. A.S., C.X. and W.S. reviewed and commented on the manuscript.

Funding

This work was supported by China Scholar Council (201908120132), the Doctoral Programme in Chemical and Process Engineering at Åbo Akademi University and Business Finland Project (43674/31/2020).

CRediT authorship contribution statement

Liu Rui: Conceptualization, Data curation, Formal analysis, Investigation, Methodology, Writing – original draft. **Smeds Annika:** Methodology, Writing – review & editing. **Willför Stefan:** Supervision, Writing – review & editing. **Xu Chunlin:** Conceptualization, Project administration, Supervision, Validation, Writing – review & editing.

Declaration of Competing Interest

The authors declare that they have no known competing financial interests or personal relationships that could have appeared to influence the work reported in this paper.

Data availability

Data will be made available on request.

Appendix A. Supporting information

Supplementary data associated with this article can be found in the online version at doi:10.1016/j.indcrop.2024.118055.

References

A.olm, T., 1981. Extended delignification by combination of modified kraft pulping and oxygen bleaching. Pap. Ja Puu 63, 315–326.

Abbadessa, A., Oinonen, P., Henriksson, G., 2018. Characterization of two novel bio-based materials from pulping process side streams: ecohelix and cleanflow black lignin. BioResources 13, 277–290. https://doi.org/10.15376/biores.13.4.7606-7627.

Alekhina, M., Ershova, O., Ebert, A., Heikkinen, S., Sixta, H., 2015. Softwood kraft lignin for value-added applications: Fractionation and structural characterization. Ind. Crops Prod. 66, 220–228. https://doi.org/10.1016/j.indcrop.2014.12.021.

Beaucamp, A., Muddasar, M., Amiinu, I.S., Moraes Leite, M., Culebras, M., Latha, K., Gutiérrez, M.C., Rodriguez-Padron, D., del Monte, F., Kennedy, T., Ryan, K.M., Luque, R., Titirici, M.-M., Collins, M.N., 2022. Lignin for energy applications – state

of the art, life cycle, technoeconomic analysis and future trends. Green Chem. 24, 8193–8226. https://doi.org/10.1039/d2gc02724k.
Berglund, J., Azhar, S., Lawoko, M., Lindström, M., Vilaplana, F., Wohlert, J., Henriksson, G., 2018. The structure of galactoglucomannan impacts the degradation under alkaline conditions. Cellulose 26, 2155–2175. https://doi.org/10.1007/s10570-018-1737-z.
Chakar, F.S., Ragauskas, A.J., 2004. Review of current and future softwood kraft lignin process chemistry. Ind. Crops Prod. 20, 131–141. https://doi.org/10.1016/j.indcrop.2004.04.016.
Challinor, J.M., 2001. Review: the development and applications of thermally assisted hydrolysis and methylation reactions. J. Anal. Appl. Pyrolysis 61, 3–34. https://doi.org/10.1016/S0165-2370(01)00146-2.
Clifford, D.J., Carson, D.M., Mckinney, D.E., Bortiatynski, J.M., Hatcher, P.G., 1995. A new rapid technique for the characterization of lignin in vascular plants - thermochemolysis with tetramethylammonium hydroxide (TMAH). Org. Geochem. 23, 169–175. https://doi.org/10.1016/0146-6380(94)00109-E.
Crestini, C., Lange, H., Sette, M., Argyropoulos, D.S., 2017. On the structure of softwood kraft lignin. Green Chem. 19, 4104–4121. https://doi.org/10.1039/c7gc01812f.
Cui, C., Sun, R., Argyropoulos, D.S., 2014. Fractional precipitation of softwood kraft lignin: isolation of narrow fractions common to a variety of lignins. ACS Sustain. Chem. Eng. 2, 959–968. https://doi.org/10.1021/sc400545d.
Dang, B.T.T., Brelid, H., Theliander, H., 2016. The impact of ionic strength on the molecular weight distribution (MWD) of lignin dissolved during softwood kraft cooking in a flow-through reactor. Holzforschung 70, 495–501. https://doi.org/10.1515/hf-2015-0103.
Dessbesell, L., Paleologou, M., Leitch, M., Pulkki, R., Xu, C., 2020. Global lignin supply overview and kraft lignin potential as an alternative for petroleum-based polymers. Renew. Sust. Energ. Rev. 123 https://doi.org/10.1016/j.rser.2020.109768.
Dimmel, D., Gellerstedt, G., 2010. Chapter 10 Chemistry of Alkaline Pulping, Lignin and Lignans: Advances in Chemistry. CRC Press.
Edgar, K.J., Buchanan, C.M., Debenham, J.S., Rundquist, P.A., Seiler, B.D., Shelton, M.C., Tindall, D., 2001. Advances in cellulose ester performance and application. Prog. Polym. Sci. 26, 1605–1688. https://doi.org/10.1016/s0079-6700(01)00027-2.
Elder, T., 2014. Bond dissociation enthalpies of a pinoresinol lignin model compound. Energ. Fuel 28, 1175–1182. https://doi.org/10.1021/ef402310h.
Farhat, W., Venditti, R.A., Hubbe, M., Taha, M., Becquart, F., Ayoub, A., 2017. A review of water-resistant hemicellulose-based materials: processing and applications. ChemSusChem 10, 305–323. https://doi.org/10.1002/cssc.201601047.
Figueiredo, P., Lintinen, K., Hirvonen, J.T., Kostiainen, M.A., Santos, H.A., 2018. Properties and chemical modifications of lignin: Towards lignin-based nanomaterials for biomedical applications. Prog. Mater. Sci. 93, 233–269. https://doi.org/10.1016/j.pmatsci.2017.12.001.
Froass, P.M., Ragauskas, A.J., Jiang, J.-e, 1998. Nuclear magnetic resonance studies. 4. Analysis of residual lignin after Kraft pulping. Ind. Eng. Chem. Res. 37, 3388–3394. https://doi.org/10.1021/ie970812c.
Fu, S.Y., Lucia, L.A., 2004. TMAH-pyrolysis - gas chromatography - mass spectrometry analysis of residual lignin changes in softwood kraft pulp during oxygen delignification. Can. J. Chem. 82, 1197–1202. https://doi.org/10.1139/V04-085.
Gellerstedt, G., 2015. Softwood kraft lignin: raw material for the future. Ind. Crops Prod. 77, 845–854. https://doi.org/10.1016/j.indcrop.2015.09.040.
Gellerstedt, G., Lindfors, E.-L., 1984. Structural changes in lignin during Kraft pulping. Holzforschung 38, 151–158. https://doi.org/10.1515/hfsg.1984.38.3.151.
Gellerstedt, G., Zhang, L., 2001. Chemistry of TCF-bleaching with oxygen and hydrogen peroxide. Oxid. Delignification Chem. 61–72.
Gellerstedt, G., Lindfors, E.L., Lapierre, C., Monties, B.B., 1984. Structural changes in lignin during kraft cooking. Part 2 - Characterizatin by acidolysis. Sven. Papp. 87, 61–67.
Gellerstedt, G., Majtnerova, A., Zhang, L., 2004. Towards a new concept of lignin condensation in kraft pulping. Initial results. C. R. Biol. 327, 817–826. https://doi.org/10.1016/j.crvi.2004.03.011.
Gierer, J., 1985. Chemistry of delignification. Wood Sci. Technol. 19, 289–312. https://doi.org/10.1007/bf00350807.
Gigli, M., Crestini, C., 2020. Fractionation of industrial lignins: opportunities and challenges. Green. Chem. 22, 4722–4746. https://doi.org/10.1039/d0gc01606c.
Giummarella, N., Linden, P.A., Areskogh, D., Lawoko, M., 2020. Fractional profiling of kraft lignin structure: unravelling insights on lignin reaction mechanisms. ACS Sustain. Chem. Eng. 8, 1112–1120. https://doi.org/10.1021/acssuschemeng.9b06027.
Hansen, N.M., Plackett, D., 2008. Sustainable films and coatings from hemicelluloses: a review. Biomacromolecules 9, 1493–1505. https://doi.org/10.1021/bm800053z.
Kawamoto, H., 2017. Lignin pyrolysis reactions. J. Wood Sci. 63, 117–132. https://doi.org/10.1007/s10086-016-1606-z.
Klingberg, A., Odermatt, J., Meier, D., 2005. Influence of parameters on pyrolysis-GC/MS of lignin in the presence of tetramethylammonium hydroxide. J. Anal. Appl. Pyrolysis 74, 104–109. https://doi.org/10.1016/j.jaap.2004.11.023.
Kuroda, K., 2000. Analytical pyrolysis products derived from cinnamyl alcohol-end groups in lignins. J. Anal. Appl. Pyrolysis 53, 123–134. https://doi.org/10.1016/S0165-2370(99)00067-4.
Kuroda, K., Nakagawa-Izumi, A., Dimmel, D.R., 2002. Pyrolysis of lignin in the presence of tetramethylammonium hydroxide (TMAH): products stemming from beta-5 substructures. J. Agric. Food Chem. 50, 3396–3400. https://doi.org/10.1021/jf011563c.
Kuroda, K.-i, 1994. Pyrolysis of arylglycol-β-propylphenyl ether lignin model in the presence of borosilicate glass fibers. J. Anal. Appl. Pyrolysis 30, 173–182. https://doi.org/10.1016/0165-2370(94)00815-9.
Kuroda, K.-i, Nakagawa-izumi, A., 2006a. Analytical pyrolysis of lignin: products stemming from β-5 substructures. Org. Geochem 37, 665–673. https://doi.org/10.1016/j.orggeochem.2006.01.012.
Kuroda, K.-I., Dimmel, D.R., 2002. Effect of pyrofoil composition on pyrolysis of lignin. J. Anal. Appl. Pyrolysis 62, 259–271. https://doi.org/10.1016/s0165-2370(01)00124-3.
Kuroda, K.-I., Nakagawa-izumi, A., 2006b. Tetramethylammonium hydroxide (TMAH) thermochemolysis of lignin: Improvement of the distribution profile of products derived from β-aryl ether subunits. J. Anal. Appl. Pyrolysis 75, 104–111. https://doi.org/10.1016/j.jaap.2005.04.011.
Lancefield, C.S., Wienk, H.L.J., Boelens, R., Weckhuysen, B.M., Bruijnincx, P.C.A., 2018. Identification of a diagnostic structural motif reveals a new reaction intermediate and condensation pathway in kraft lignin formation. Chem. Sci. 9, 6348–6360. https://doi.org/10.1039/c8sc02000k.
Landucci, L.L., 1991. Application of modern liquid-state NMR to lignin characterization. 2.13C Signal resolution and useful techniques. Holzforschung 45, 425–432. https://doi.org/10.1515/hfsg.1991.45.6.425.
Lapierre, C., Pollet, B., Monties, B., Rolando, C., 1991. Thioacidolysis of spruce lignin: GC-MS analysis of the main dimers recovered after Raney Nickel desulphuration. Holzforschung 45, 61–68. https://doi.org/10.1515/hfsg.1991.45.1.61.
Lawoko, M., Berggren, R., Berthold, F., Henriksson, G., Gellerstedt, G., 2004. Changes in the lignin-carbohydrate complex in softwood kraft pulp during kraft and oxygen delignification. Holzforschung 58, 603–610. https://doi.org/10.1515/hf.2004.114.
Lawoko, M., Henriksson, G., Gellerstedt, G., 2005. Structural differences between the lignin-carbohydrate complexes present in wood and in chemical pulps. Biomacromolecules 6, 3467–3473. https://doi.org/10.1021/bm058014q.
Liu, R., Dai, L., Xu, C., Wang, K., Zheng, C., Si, C., 2020. Lignin-based micro-and nanomaterials and their composites in biomedical applications. ChemSusChem 13, 4266–4283. https://doi.org/10.1002/cssc.202000783.
Liu, R., Smeds, A., Wang, L.Y., Pranovich, A., Hemming, J., Willfor, S., Zhang, H.B., Xu, C.L., 2021. Fractionation of lignin with decreased heterogeneity: based on a detailed characteristics study of sequentially extracted softwood kraft lignin. ACS Sustain. Chem. Eng. 9, 13862–13873. https://doi.org/10.1021/acssuschemeng.1c04725.
Liu, R., Smeds, A., Tirri, T., Zhang, H.B., Willfor, S., Xu, C.L., 2022. Influence of carbohydrates covalently bonded with lignin on solvent fractionation, thermal properties, and nanoparticle formation of lignin. ACS Sustain. Chem. Eng. 10, 14588–14599. https://doi.org/10.1021/acssuschemeng.2c04498.
Ljunggren, S., 1980. The significance of aryl ether cleavage in kraft delignification of softwood. Sven. Papp. 83, 363–369.
Mattsson, C., Hasani, M., Dang, B., Mayzel, M., Theliander, H., 2017. About structural changes of lignin during kraft cooking and the kinetics of delignification. Holzforschung 71, 545–553. https://doi.org/10.1515/hf-2016-0190.
McKinney, D.E., Carson, D.M., Clifford, D.J., Minard, R.D., Hatcher, P.G., 1995. Off-line thermochemolysis versus flash pyrolysis for the in situ methylation of lignin: Is pyrolysis necessary? J. Anal. Appl. Pyrolysis 34, 41–46. https://doi.org/10.1016/0165-2370(94)00865-x.
Nguyen, N.A., Barnes, S.H., Bowland, C.C., Meek, K.M., Littrell, K.C., Keum, J.K., Naskar, A.K., 2018. A path for lignin valorization via additive manufacturing of high-performance sustainable composites with enhanced 3D printability. Sci. Adv. 4, eaat4967 https://doi.org/10.1126/sciadv.aat4967.
Novo, L.P., Curvelo, A.A.S., 2019. Hansen solubilityparameters: a tool for solvent selection for organosolv delignification. Ind. Eng. Chem. Res 58, 14520–14527. https://doi.org/10.1021/acs.iecr.9b00875.
Önnerud, H., 2002. On the structure of native softwood and hardwood lignins, Department of pulp and paper technolog. Royal institute of Technology, KTH, Stockholm.
Reale, S., Di Tullio, A., Spreti, N., De Angelis, F., 2004. Mass spectrometry in the biosynthetic and structural investigation of lignins. Mass Spectrom. Rev. 23, 87–126. https://doi.org/10.1002/mas.10072.
Rodrigues, J.S., Lima, V., Araújo, L.C.P., Botaro, V.R., 2021. Lignin fractionation methods: can lignin fractions be separated in a true industrial process? Ind. Eng. Chem. Res 60, 10863–10881. https://doi.org/10.1021/acs.iecr.1c01704.
Sadeghifar, H., Ragauskas, A., 2020. Perspective on technical lignin fractionation. ACS Sustain. Chem. Eng. 8, 8086–8101. https://doi.org/10.1021/acssuschemeng.0c01348.
Schuerch, C., 1952. The solvent properties of liquids and their relation to the solubility, swelling, isolation and fractionation of lignin. J Am Chem Soc 74, 5061–5067. DOI 10.1021/ja01140a020.
Seabra, A.B., Bernardes, J.S., Favaro, W.J., Paula, A.J., Duran, N., 2018. Cellulose nanocrystals as carriers in medicine and their toxicities: a review. Carbohydr. Polym. 181, 514–527. https://doi.org/10.1016/j.carbpol.2017.12.014.
Shadkami, F., Helleur, R., 2010. Recent applications in analytical thermochemolysis. J. Anal. Appl. Pyrolysis 89, 2–16. https://doi.org/10.1016/j.jaap.2010.05.007.
Shen, X., Xin, Y., Liu, H., Han, B., 2020. Product-oriented direct cleavage of chemical linkages in lignin. ChemSusChem 13, 4367–4381. https://doi.org/10.1002/cssc.202001025.
Smeds, A.I., Češková, I., Eklund, P.C., Willför, S.M., 2012. Identification of new lignans in Norway spruce knotwood extracts. Holzforschung 66, 553–567. https://doi.org/10.1515/hf-2011-0218.
Supriyanto, Usino, D.O., Ylitervo, P., Dou, J.Z., Sipponen, M.H., Richards, T., 2020. Identifying the primary reactions and products of fast pyrolysis of alkali lignin. J. Anal. Appl. Pyrolysis 151. https://doi.org/10.1016/j.jaap.2020.104917.
Tanczos, I., Rendl, K., Schmidt, H., 1999. The behavior of aldehydes—produced as primary pyrolysis products—in the thermochemolysis with tetramethylammonium

hydroxide. J. Anal. Appl. Pyrolysis 49, 319–327. https://doi.org/10.1016/s0165-2370(98)00132-6.
Tricker, A.W., Stellato, M.J., Kwok, T.T., Kruyer, N.S., Wang, Z., Nair, S., Thomas, V.M., Realff, M.J., Bommarius, A.S., Sievers, C., 2020. Similarities in recalcitrant structures of industrial non-Kraft and Kraft Lignin. ChemSusChem 13, 4624–4632. https://doi.org/10.1002/cssc.202001219.
Upton, B.M., Kasko, A.M., 2016. Strategies for the conversion of lignin to high-value polymeric materials: review and perspective. Chem. Rev. 116, 2275–2306. https://doi.org/10.1021/acs.chemrev.5b00345.
Wang, Y.Y., Li, M., Wyman, C.E., Cai, C.M., Ragauskas, A.J., 2018. Fast fractionation of technical lignins by organic cosolvents. ACS Sustain. Chem. Eng. 6, 6064–6072. https://doi.org/10.1021/acssuschemeng.7b04546.
Zhang, L., Henriksson, G., Gellerstedt, G., 2003. The formation of beta-beta structures in lignin biosynthesis–are there two different pathways? Org. Biomol. Chem. 1, 3621–3624. https://doi.org/10.1039/b306434d.